The DEAD-box RNA Helicase RH50 Is a 23S-4.5S rRNA Maturation Factor that Functionally Overlaps with the Plastid Signaling Factor GUN1[1][OPEN]

Francesca Paieri,[a,b,2] Luca Tadini,[a,2] Nikolay Manavski,[2] Tatjana Kleine,[a] Roberto Ferrari,[c] Piero Morandini,[c] Paolo Pesaresi,[d] Jörg Meurer,[a] and Dario Leister[a,3]

[a]Plant Molecular Biology, Faculty of Biology, Ludwig-Maximilians-Universität München, D-82152 Planegg-Martinsried, Germany
[b]Centro Ricerca e Innovazione, Fondazione Edmund Mach, I-38010, San Michele all'Adige, Italy
[c]Department of Biosciences, I-20133 Milano, Università degli studi di Milano, Italy
[d]Department of Agricultural and Environmental Sciences — Production, Landscape, Agroenergy, I-20133 Milano, Università degli studi di Milano, Italy

ORCID IDs: 0000-0003-2315-7695 (L.T.); 0000-0003-2740-5991 (N.M.); 0000-0001-6455-3470 (T.K.); 0000-0003-4015-8104 (R.F.); 0000-0002-7994-6426 (P.M.); 0000-0002-3236-7005 (P.P.); 0000-0003-2973-9514 (J.M.); 0000-0003-1897-8421 (D.L.).

DEAD-box RNA helicases (DBRHs) modulate RNA secondary structure, allowing RNA molecules to adopt the conformations required for interaction with their target proteins. RH50 is a chloroplast-located DBRH that colocalizes and is coexpressed with GUN1, a central factor in chloroplast-to-nucleus signaling. When combined with mutations that impair plastid gene expression (*prors1-1*, *prpl11-1*, *prps1-1*, *prps21-1*, *prps17-1*, and *prpl24-1*), *rh50* and *gun1* mutations evoke similar patterns of epistatic effects. These observations, together with the synergistic growth phenotype of the double mutant *rh50-1 gun1-102*, suggest that RH50 and GUN1 are functionally related and that this function is associated with plastid gene expression, in particular ribosome functioning. However, *rh50-1* itself is not a gun mutant, although—like *gun1-102*—the *rh50-1* mutation suppresses the down-regulation of nuclear genes for photosynthesis induced by the *prors1-1* mutation. The RH50 protein comigrates with ribosomal particles, and is required for efficient translation of plastid proteins. RH50 binds to transcripts of the 23S-4.5S intergenic region and, in its absence, levels of the corresponding rRNA processing intermediate are strongly increased, implying that RH50 is required for the maturation of the 23S and 4.5S rRNAs. This inference is supported by the finding that loss of RH50 renders chloroplast protein synthesis sensitive to erythromycin and exposure to cold. Based on these results, we conclude that RH50 is a plastid rRNA maturation factor.

DEAD-box RNA helicases (DBRHs) contain at least nine conserved motifs that constitute the helicase core domain, including the stretch of highly conserved Asp-Glu-Ala-Asp (D-E-A-D) residues in motif II that gave this protein family its name (Caruthers and McKay, 2002; Cordin et al., 2006). DBRHs participate in many cellular processes, including RNA metabolism (synthesis, modification, cleavage, and degradation), ribosome biogenesis, and translation initiation (Silverman et al., 2003; Cordin et al., 2006). RNA molecules must fold into specific conformations to interact with proteins, and DBRHs facilitate the remodeling of RNA secondary structure by unwinding duplexes in a localized strand separation reaction (Jarmoskaite and Russell, 2011). To this end, the helicase binds to the duplex region, interacts with one end of the duplex and then uses energy from cycles of ATP binding and hydrolysis to translocate directionally along one of the strands while displacing the other (Jarmoskaite and Russell, 2011). Recent data suggest that DBRHs have distinct activities compared to other superfamily 2 (SF2) RNA helicase proteins, and often do not show the same unwinding activity as observed for other SF2 RNA helicases (Jarmoskaite and Russell, 2014).

In all, 58 DBRHs have been annotated in the Arabidopsis (*Arabidopsis thaliana*) genome (Mingam et al., 2004), 10 of which (RH3, 11, 17, 22, 26, 33, 41, 50, 52, and 58) are predicted to be plastid-localized (Asakura et al., 2012). Mass spectrometry analyses have meanwhile confirmed the presence of seven DBRHs in Arabidopsis chloroplasts, namely RH3, 22, 26, 39, 47, 50, and 58 (Olinares et al., 2010; Majeran et al., 2012). Phylogenetic analyses cluster the plastid DBRHs into several groups: RH3 is assigned to a

[1] This work was supported by the Deutsche Forschungsgemeinschaft (TRR 175, projects A03, C01, and C05).

[2] These authors contributed equally to the article.

[3] Address correspondence to leister@lmu.de.

The author responsible for distribution of materials integral to the findings presented in this article in accordance with the policy described in the Instructions for Authors (www.plantphysiol.org) is: Dario Leister (leister@lmu.de).

D.L. conceived the research plan. J.M., P.P., and D.L. supervised the experiments; F.P., L.T., N.M., T.K., R.F., and P.M. performed and analyzed the experiments; F.P. wrote the manuscript with contributions from all authors; D.L. supervised the writing process and prepared the final version.

[OPEN] Articles can be viewed without a subscription.

www.plantphysiol.org/cgi/doi/10.1104/pp.17.01545

subset with mitochondrial and nuclear orthologs, RH26 belongs to a clade containing proteins of unknown function, and RH22, RH39, RH47, RH50, and RH58 form a separate group (Asakura et al., 2012; Chi et al., 2012). Some of the plastid helicases have been functionally characterized. The *rh39* mutant accumulates precursors of the 23S rRNA, indicating that RH39 is involved in plastid rRNA maturation, and is required to introduce the hidden break into the 23S rRNA (Nishimura et al., 2010). RH22 is also involved in the assembly of the 50S ribosomal subunit in the chloroplast: complete loss of RH22 function is lethal, whereas a knockdown line displayed delayed cotyledon greening and aberrant accumulation of the precursor of the 23S and 4.5S chloroplast rRNAs (Chi et al., 2012). Yeast two-hybrid (Y2H) and pull-down assays indicated that RH22 interacts with PRPL24 in the 50S ribosomal subunit and with a short fragment of the 23S rRNA. RH3 has been characterized in both Arabidopsis and maize (*Zea mays*; Asakura et al., 2012; Gu et al., 2014). The *atrh3* null mutant is embryo-lethal, whereas a weak allele (*atrh3-4*) resulted in pale-green seedlings due to defects in splicing of group-II introns and reduced levels of the 50S ribosomal subunit owing to impaired production of 23S and 4.5S rRNAs (Asakura et al., 2012; Gu et al., 2014). A tobacco (*Nicotiana benthamiana*) *RH58/VDL* mutant is defective in plastid differentiation and plant morphogenesis (Wang et al., 2000). The rice (*Oryza sativa*) homolog of Arabidopsis RH50 (OsBIRH1) exhibits RNA helicase activity in vitro, but no direct target of OsBIRH1 has yet been identified (Li et al., 2008).

In Arabidopsis, RH50 was detected in association with the transcriptionally active chromosome of the plastid (pTAC), together with plastid ribosomal proteins (PRPs), the PEP core enzyme, and proteins involved in transcription, translation, and RNA metabolism, including RNases and DBRHs (Olinares et al., 2010; Majeran et al., 2012). Helical repeat proteins, such as octatricopeptide, pentatricopeptide (PPRs), and tetratricopeptide repeat proteins were also identified in the pTAC complex, in agreement with their primary roles in modulating gene transcription and RNA editing, maturation, and stability. Among the PPR proteins identified in the pTAC is the product of *GENOMES UNCOUPLED1* (GUN1) (Koussevitzky et al., 2007). GUN1 integrates information transmitted by several retrograde signaling pathways (Koussevitzky et al., 2007) and physically interacts with several other chloroplast proteins involved in chloroplast protein homeostasis (Tadini et al., 2016). Chlorophyll *A/B*-Binding Overexpression1 (COE1)/mTERF4 was recently proposed to form part of a GUN1-mediated retrograde signaling pathway (Sun et al., 2016). Because the *coe1* mutant accumulates high levels of unprocessed RNAs, it was speculated that these unprocessed RNAs might represent a retrograde signal for the down-regulation of nuclear photosynthetic gene expression (Sun et al., 2016).

Prompted by the observation that the chloroplast DBRH RH50 and GUN1 have similar expression profiles, we have studied the role of RH50 in plastid gene expression (PGE) and its relationship to GUN1 and retrograde signaling. RH50 promotes the maturation of plastid 23S and 4.5S rRNAs. Moreover, when combined with other mutations affecting PGE, *rh50* in large measure phenocopies *gun1*. These findings imply that GUN1 might also function in the regulation of plastid ribosome biogenesis.

RESULTS

RH50 and GUN1: Coexpression and Colocalization

We employed a guilt-by-association approach to identify candidate genes involved in plastid protein homeostasis and plastid signaling based on their coexpression with *GUN1*. As part of this effort, mRNA expression data for all predicted plastid-located DBRHs encoded in the Arabidopsis nuclear genome were compared with the results for the *GUN1* coexpression cluster (as described in "Materials and Methods"), which itself includes the genes for the plastid ribosomal protein S1 (*PRPS1*), two tetrapyrrole biosynthesis enzymes (the protoporphyrinogen oxidase (*PPOX*), and the D subunit of the magnesium chelatase (*CHLD*), as well as a set of proteins involved in plastid protein homeostasis (Tadini et al., 2016). This allowed us to identify *RH50* as the chloroplast DBRH gene with the highest degree of coexpression with *GUN1*, *PPOX*, and *CHLD* (Fig. 1A), followed by *RH58*. Two additional coexpression clusters are formed by *RH17*, *RH22*, and *RH26*, and by *RH11* and *RH52*. The predicted chloroplast DHBRs RH3, RH33, and RH41 could not be included in this analysis, because they are not represented on the ATH1 Affymetrix Array.

Not only are *RH50* and *GUN1* coregulated, their products were previously shown to be located in pTACs, together with several other DBRHs and components of the protein expression machinery (Koussevitzky et al., 2007; Olinares et al., 2010). To confirm the colocalization of RH50 and GUN1 in pTACs, GUN1-RFP and RH50-GFP protein fusions were transiently coexpressed in Arabidopsis protoplasts (see "Materials and Methods"). The GFP and RFP signals could be clearly detected as overlapping fluorescence foci within chloroplasts (Fig. 1B), indicating that RH50 and GUN1 are found in the same subcompartment.

rh50 Is Not a *gun* Mutant but, Like *gun1*, Suppresses Transcriptional Down-Regulation of Photosynthesis-Associated Nuclear Genes

Because *RH50* and *GUN1* are coregulated at the mRNA level and their products are located in the same chloroplast subcompartment, we investigated whether, like GUN1 (Tadini et al., 2016), RH50 plays a role in retrograde signaling and plastid protein homeostasis. To this end, two independent loss-of-function alleles of *RH50* (*rh50-1* and *rh50-2*; Fig, 2A, and "Materials and Methods") were isolated. In *rh50-1* mutant plants, the mutation is caused by a T-DNA insertion, whereas in *rh50-2* a transposon is inserted in the *RH50* gene. Both insertions are

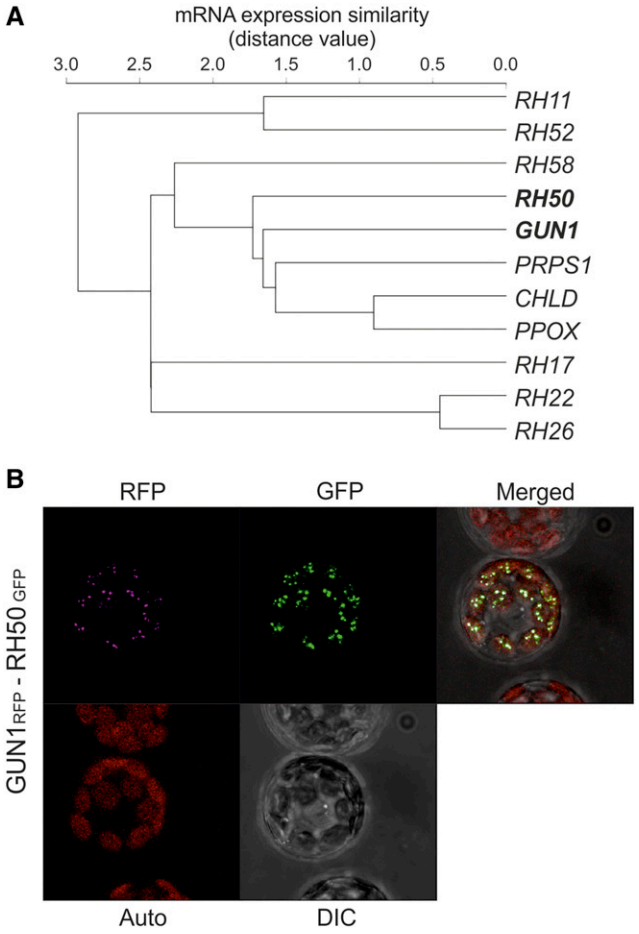

Figure 1. *RH50* and *GUN1* are coexpressed and their products colocalize in chloroplasts. A, Coexpression analysis. Among genes coding for chloroplast-localized DBRHs, *RH50* shows the highest coregulation score with *GUN1*. Correlations between the *GUN1* expression pattern and those of all putative chloroplast-localized DEAD box RNA helicases genes were hierarchically clustered (see "Materials and Methods"). As a measure of coexpression, *PRPS1*, and *CHLD* and *PPOX* (that encode two enzymes in the tetrapyrrole biosynthesis pathway), which are among the top *GUN1* coexpressors (Tadini et al., 2016), were included. *RH3*, *RH33*, and *RH41* are not represented on the Affymetrix array used in our analysis. Degrees of coexpression were measured by the mutual rank method. Low distance values indicate high coexpression. Full names and accession numbers of corresponding proteins encoded are provided in "Materials and Methods". All gene products are predicted or experimentally confirmed chloroplast proteins. B, RH50 and GUN1 colocalize in chloroplasts. Protoplasts from 2-week-old Arabidopsis cotyledons were isolated (as described in "Material and Methods") and cotransfected with GUN1-RFP and RH50-GFP constructs. The RFP signal (red fluorescence) clearly overlapped with the GFP signal (green fluorescence) within the chloroplast. Fluorescence was imaged by confocal microscopy.

located in the second exon and completely prevent expression of the RH50 protein (Fig. 2B). The possible involvement of RH50 in GUN1-mediated retrograde signaling was analyzed by testing whether *rh50-1* seedlings exhibit the *genomes uncoupled* (*gun*) phenotype, i.e. aberrant *LHCB1* expression in the presence of norflurazon (NF) or lincomycin (LIN; Fig. 2C). However, as in the wild type, *LHCB1* expression was strongly reduced in the *rh50-1* single mutant after treatment with NF or LIN, whereas in *gun1-102* plants, *LHCB1* expression was derepressed. Moreover, in the *rh50-1 gun1-102* double mutant, the *gun* phenotype was unchanged.

To further investigate the involvement of RH50 in PGE-mediated retrograde signaling in adult plants, *rh50-1* was crossed into the *prors1-1* genetic background and the expression of photosynthesis-associated nuclear genes (PhANGs) was assessed (Fig. 2D). The *prors1-1* mutation down-regulates mRNA expression of the Pro tRNA synthetase1, thereby perturbing PGE in adult plants (Pesaresi et al., 2006). Interestingly, the expression of *LHCA3*, *LHCA4*, *LHCB1*, *PSAO*, and *PSAK* genes, which is down-regulated by approximately 20% to 30% in the *prors1-1* mutant, was restored to wild-type-like levels in *rh50-1 prors1-1* mutant, as in the case of the *gun1-102 prors1-1* double mutant (Tadini et al., 2016).

Thus, like GUN1, RH50 is capable of modulating chloroplast-to-nucleus communication when the PGE machinery is mildly disrupted in mature plants, as in case of *prors1-1*. However, in seedlings and under more severe conditions, such as those induced by treatment with NF or LIN, only GUN1 appears to be critical for plastid signaling.

rh50 and *gun1* Mutations Display Similar Patterns of Epistasis when Combined with Mutations Affecting PGE

Both synergistic enhancer (*gun1-102 prpl11-1*) and suppressor (*gun1-102 prps1-1*) phenotypes have been observed when the *gun1* mutation was introduced into genetic backgrounds carrying mutations in genes for plastid ribosomal proteins (Tadini et al., 2016). These findings pointed to a functional link between GUN1 and plastid ribosomes. Therefore, to further compare the effects of the *rh50-1* and *gun1-102* mutations on chloroplast function, double mutants combining *rh50-1* or *gun1-102* with several other mutations (*prors1-1*, *prpl11-1*, *prps1-1*, *prps21-1*, *prps17-1*, and *prpl24-1*) were generated and characterized (Fig. 3, A to F). In contrast to Arabidopsis plants defective for RH3, 22, or 39, which are characterized by developmental arrest at the embryo stage (Nishimura et al., 2010; Asakura et al., 2012; Chi et al., 2012), both *rh50* mutant alleles behaved like wild type with respect to plant size and photosynthetic performance [measured as effective quantum yield of photosystem II (Φ_{II}) after a 15-min exposure to actinic light of 37 μmol photons m^{-2} s^{-1}; see "Materials and Methods"] under standard growth conditions (Fig. 3A). Interestingly, *rh50-1 gun1-102* plants were markedly smaller than either of the single mutants (Fig. 3, A and B), supporting the idea of a functional interaction between *GUN1* and *RH50*, although the photosynthetic performance of adult plants was unaffected.

Like *gun1-102*, *rh50-1* restored PhANG expression in the *prors1-1* genetic background (see Fig. 2D). In both cases, this restoration of PhANG expression was associated with increased plant size and improved photosynthetic performance (Φ_{II} of 0.73 $\pm$ 0.02 for both

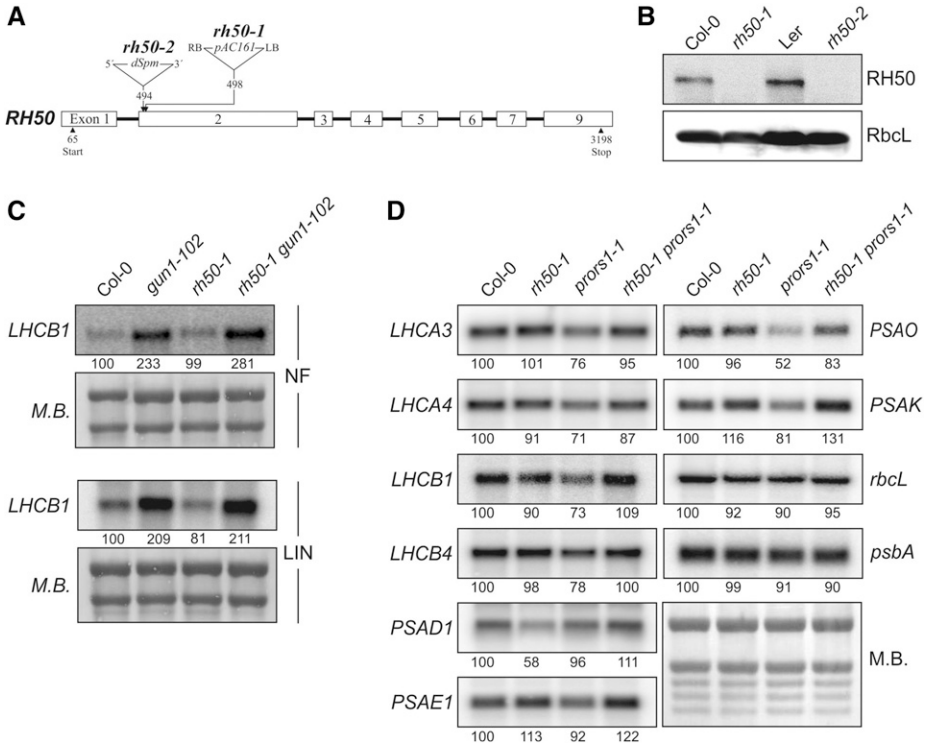

Figure 2. RH50 and regulation of PhANG expression. A, Schematic representations of the *RH50* mutant alleles. The *rh50-1* and *rh50-2* mutations are due to the insertion of a T-DNA and a transposon, respectively. Left borders and right borders indicate the orientation of the T-DNA, 5′ and 3′ that of the transposon. Numbered boxes symbolize the exons and black lines the introns. Start and stop codons are indicated. B, Immunoblot analysis of total proteins extracted from wild-type (Col-0 and L*er*), *rh50-1*, and *rh50-2* plants was performed with antibodies specific for RH50 (see "Materials and Methods") and, as a control, RbcL. C, Assay for the *gun* phenotype. RNA gel-blot analysis of *LHCB1.2* expression was carried out using total RNA isolated from wild-type (Col-0) and mutant (*gun1-102*, *rh50-1*, and *rh50-1 gun1-102*) seedlings grown for 10 d in the presence of norflurazon or lincomycin. D, PhANG expression in wild-type (Col-0) and mutant (*gun1-102*, *rh50-1*, and *rh50-1 gun1-102*) plants. Transcripts of nuclear (*LHCA3*, *LHCA4*, *LHCB1*, *LHCB4*, *PSAD1*, *PSAE1*, *PSAO*, and *PSAK*) and plastid (*rbcL* and *psbA*) genes encoding photosynthetic functions, isolated from light-adapted wild-type (Col-0), *rh50-1*, *prors1-1*, and *rh50-1 prors1-1* plants, were quantified by RNA gel-blot analysis. Blots were stained with Methylene Blue to assess RNA loading. Quantification of signals (by the software ImageJ) relative to Col-0 (= 100%) is provided below each panel. LB, left borders; RB, right borders; M.B., Methylene Blue; NF, norflurazon; LIN, lincomycin.

double mutants versus 0.68 ± 0.02 in *prors1-1*) relative to the *prors1-1* single mutant (Fig. 3C).

The *rh50* and *gun1-102* mutant alleles were also combined with mutations affecting proteins of the 30S (*prps1-1*, *prps17-1*, and *prps21-1*) and 50S (*prpl11-1* and *prpl24-1*) subunits of the plastid ribosome. The *rh50-1* mutation partially suppressed the effects of the leaky *prps1-1* mutation on photosynthetic performance, albeit not to the same extent as *gun1-102* (*prps1-1*, 0.49 ± 0.02; *rh50-1 prps1-1*, 0.54 ± 0.02; *gun1-102 prps1-1*, 0.66 ± 0.02), whereas *gun1-102 prps1-1* double mutants have larger plant sizes than *prps1-1* plants (Tadini et al., 2016; Fig. 3C). As in the case of the *gun1-102 prps1-1* double mutant (Tadini et al., 2016), the improvement of photosynthetic parameters in the *rh50-1 prps1-1* mutant was associated with increased amounts of PRPS1 protein, from approximately 40% of the wild-type level in the leaky *prps1-1* single mutant to approximately 75% in the *rh50-1 prps1-1* mutant background (Fig. 3D). Complete loss of *GUN1* was previously shown to restore wild-type-like PRPS1 protein levels in the *prps1-1* background (Tadini et al., 2016). Because the leaky *prps1-1* mutation was due to a T-DNA insertion in the promoter region of the *PRPS1* gene (Romani et al., 2012) that led to a decrease in the accumulation of *PRPS1* transcripts equally in *prps1-1* and *prps1-1 gun1-102* plants, it was previously concluded that GUN1 has a role in protein homeostasis in chloroplasts by contributing to decrease the stability of chloroplast proteins like PRPS1 (Tadini et al., 2016). Consequently, also RH50 might have a role, either directly or indirectly, in PRPS1 homeostasis.

Of the other two mutations for 30S ribosomal proteins tested, one behaved identically and the other discordantly in *rh50-1* and *gun1-102* backgrounds. Whereas *rh50-1 prps21-1* and *gun1-102 prps21-1* had phenotypes very similar to the *prps21-1* single mutant in terms of plant size and photosynthetic efficiency (Fig. 3C), the phenotype of *rh50-2 prps17-1* differed markedly from that of *gun1-102 prps17-1*. The former was

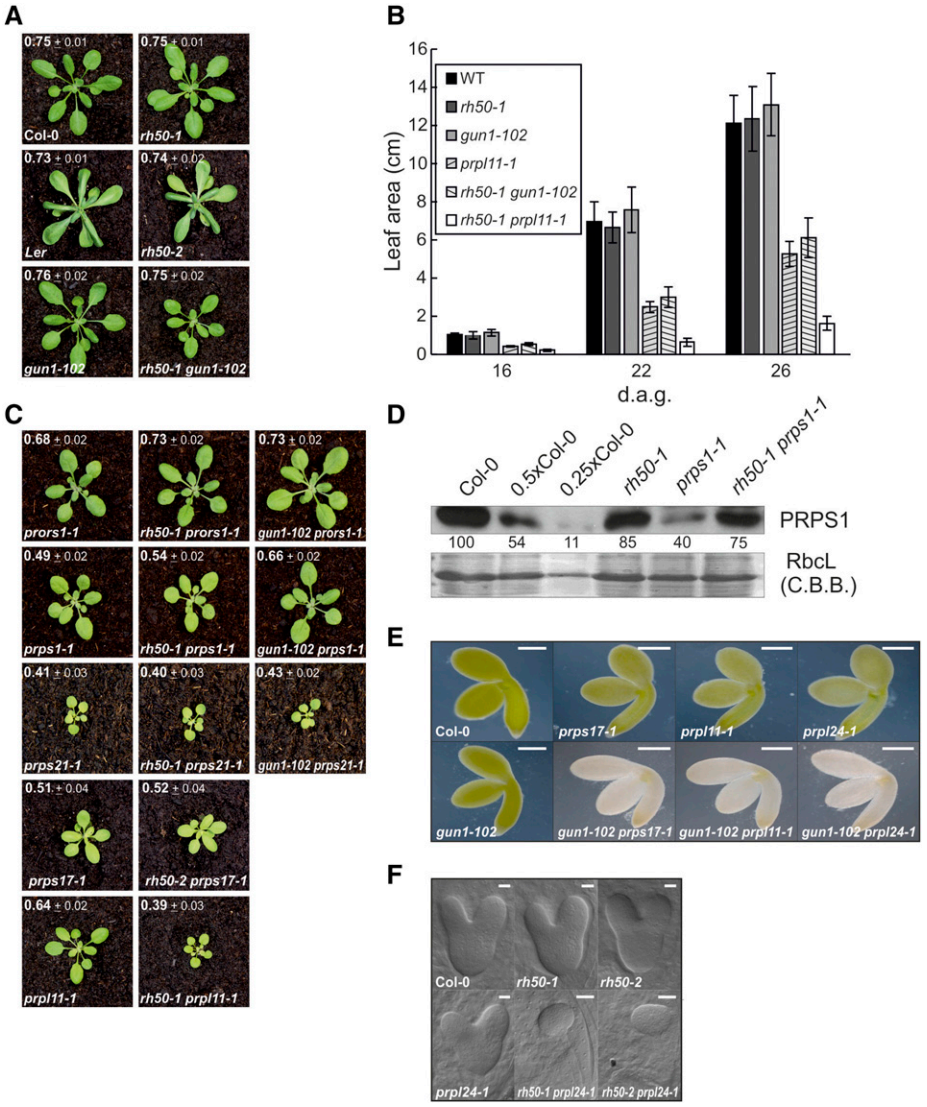

Figure 3. Genetic interactions between *rh50* or *gun1* and mutations (*prors1-1*, *prpl11-1*, *prps1-1*, *prps21-1*, *prps17-1*, and *prpl24-1*) affecting PGE. A, Phenotypes of 26-d-old wild type (Col-0 and L*er*), single (*rh50-1*, *rh50-2*, and *gun1-102*) mutants, and double (*rh50-1 gun1-102*) mutant plants exposed to 80 μmol photons m^{-2} s^{-1} under long-day conditions in a climate chamber. The effective quantum yield of photosystem II (Φ_{II}), measured after a 15-min exposure to actinic light of 37 μmol photons m^{-2} s^{-1} (see "Materials and Methods"), was determined for each genotype (average ± SD; $n \geq 12$). B, Growth kinetics of wild type (Col-0), *rh50-1*, *gun1-102*, *prpl11-1*, *rh50-1 gun1-102*, and *rh50-1 prpl11-1* were measured at 16, 22, and 26 d after germination. For each time point, the average leaf area was measured ($n \geq 15$). C, Phenotypes of single (*prors1-1*, *prpl11-1*, *prps1-1*, *prps21-1*, *rh50-2*, and *prps17-1*) and double (*rh50-1 prors1-1*, *gun1-102 prors1-1*, *rh50-1 prpl11-1*, *rh50-1 prps1-1*, *gun1-102 prps1-1*, *rh50-1 prps21-1*, *gun1-102 prps21-1*, and *rh50-2 prps17-1*) mutant plants grown and analyzed as in (A). D, Loss of RH50 partially suppresses the reduction in the level of PRPS1 protein seen in the *prps1-1* background. An immunoblot analysis was performed with a PRPS1-specific antibody on extracts of the wild type (Col-0), *rh50-1*, and *prps1-1* single mutants and the *rh50-1 prps1-1* double mutant. To assess loading levels, blots were stained with Coomassie Brilliant Blue, and quantification of signals (by the software ImageJ) relative to the wild type (100%) is provided. E, Images of mature embryos (bent cotyledon stage) from wild type (Col-0), single (*prpl11-1*, *prpl24-1*, *prpl17-1*, and *gun1-102*), and double (*gun1-102 prpl11-1*, *gun1-102 prpl24-1*, and *gun1-102 prpl17-1*) mutant plants. Bars = 200 μm. F, Characterization of embryo development in wild type (Col-0), single (*rh50-1*, *rh50-2*, and *prps24-1*), and double (*rh50-1 prps24-1* and *rh50-2 prps24-1*) mutant plants. In 25% of embryos from *RH50/rh50-1 prpl24-1/prpl24-1* and *RH50/rh50-2 prpl24-1/prpl24-1* siliques, development ceased at the (disordered) globular stage. Bars = 20 μm. C.B.B., Coomassie Brilliant Blue; d.a.g., days after germination.

indistinguishable from the *prps17-1* mutant (Romani et al., 2012), showing reduced plant size and reduced photosynthesis compared to the wild type (Fig. 3C), whereas *gun1-102 prps17-1* plants were seedling lethal (Fig. 3E). Even more severe effects were observed when *rh50-1* or *gun1-102* was crossed into backgrounds defective for 50S ribosomal proteins (*prpl11-1* and *prpl24-1*). Whereas *gun1-102 prpl11-1* plants were seedling-lethal (Tadini et al., 2016; Fig. 3E), the *rh50-1 prpl11-1* double mutant was viable when grown on soil but strongly affected, relative to the *prpl11-1* single mutant, in terms of growth rate and photosynthesis (Fig. 3, B and C). The combination of *rh50-1* with *prpl24-1* resulted in embryo lethality (Fig. 3F), whereas *gun1-102 prpl24-1* plants were seedling-lethal (Fig. 3E). Growth arrest at the globular stage of embryo development has been reported for several other mutants deficient in plastid ribosomal proteins (like *prps20*, *prpl1*, *prpl4*, *prpl21*, *prpl27*, or *prpl35*; Romani et al., 2012; Yin et al., 2012).

Taken together, these analyses suggest that the loss of *RH50*, like that of *GUN1*, generally tends to potentiate the effects of mutations in genes for plastid ribosomal subunits (such as *prors1*, *prps1*, *prps21*, *prpl11*, and *prpl24*). However, loss of *GUN1* provoked more dramatic effects in two cases (*prps1-1* and *prpl11-1*), and only in combination with the *prpl24-1* mutation did the loss of *RH50* lead to a stronger effect than loss of *GUN1*. Moreover, in contrast to *gun1-102*, *rh50-1* did not enhance the *prp17-1* phenotype.

These findings imply that many of the epistatic effects of *gun1* in backgrounds containing mutations affecting PGE are not unique. Clearly, both RH50 and GUN1 can mitigate the effects of partial loss of some ribosomal functions at least under the conditions studied here.

Functional and Physical Association of RH50 with the Plastid Ribosome

As described above, the strongest epistatic effects of *rh50-1* were observed on mutations in genes for subunits of the large plastid ribosomal subunit (see Fig. 3). To determine whether ribosomes are structurally impaired in the *rh50-1* mutant, we analyzed mutant and wild-type responses to the antibiotics chloramphenicol, LIN, and erythromycin, which are known to target the large subunit of the plastid ribosome and prevent elongation of the nascent polypeptide chain, either by binding to the peptidyltransferase center (chloramphenicol and LIN) or by blocking the exit tunnel (erythromycin; Sohmen et al., 2009). The *rh50-1* mutant showed a wild-type-like phenotype when treated with LIN and chloramphenicol, but was clearly more sensitive to erythromycin, as mutant seedlings were smaller and paler than, and exhibited reduced photosynthetic efficiency relative to, wild-type seedlings (Fig. 4A).

Defects in plastid translational capacity are often associated with impaired acclimation to cold, as reported previously in mutants defective for *PRPL33*, *PRPS5*, or *RDB1* (Rogalski et al., 2008; Wang et al., 2016; Zhang et al., 2016). Therefore, we quantified cold acclimation in both *rh50-1* mutants and wild-type plants. Under standard growth conditions, 7-d-old *rh50-1* mutant seedlings showed a reduction in maximum quantum yield of photosystem II compared to the wild type (F_V/F_M 0.67 $\pm$ 0.01 versus 0.77 $\pm$ 0.01, respectively; Fig. 4B), a phenotype that is lost in adult plants (see Fig. 3A). Intriguingly, *rh50-1* mutants are less tolerant than wild type to cold stress. In *rh50-1* seedlings, germinated and grown on Murashige & Skoog (MS) medium supplemented with 1% Suc for 6 weeks at 4°C and then transferred to 22°C, growth rate, chlorophyll accumulation, and F_V/F_M (*rh50-1*: 0.27 $\pm$ 0.07; wild type: 0.72 $\pm$ 0.02) were all adversely affected (Fig. 4B). In the absence of Suc, this phenotype was exacerbated, as *rh50-1* mutants completely failed to accumulate chlorophyll, and died as seedlings (Supplemental Fig. S1). Furthermore, reducing the light intensity to lessen oxidative stress (see "Materials and Methods") failed to rescue cold-treated *rh50-1* seedlings (Supplemental Fig. S1).

To investigate whether RH50 physically interacts with plastid ribosomal proteins, Y2H assays were performed. In these experiments, RH50 was employed as bait (Bd vector) and tested for binding to GUN1, PRPL11, PRPL24, PRPS1, PRPS17, and PRPS21 as prey proteins (Ad vectors). Apart from the previously described $GUN1^{BD}$-$CHLD^{AD}$ interaction (Tadini et al., 2016), used as positive control, no further binding interactions were detected (see Supplemental Fig. S2).

To test whether RH50 associates with intact ribosomes in vivo, size-exclusion chromatography of soluble chloroplast stroma extracts was conducted. As previously described (Olinares et al., 2010), RH50 was identified in megadalton complexes (with a main peak in fractions 5 to 7), comigrating with ribosomal particles, as demonstrated by immunodetection using RH50-, PRPL11-, and PRPS5-specific antibodies (Fig. 4C). Moreover, when extracts were treated with RNase, RH50 was no longer detectable in fractions 5 to 7, indicating that the protein associates with RNA-containing and RNase-sensitive particles. A similar trend was observed for proteins of the large and small ribosomal subunit, pointing to the association of RH50 with immature ribosomes, which are more accessible for RNases than the mature forms found in fractions 3 and 4.

Thus, loss of RH50 increases sensitivity to erythromycin—an inhibitor that binds to the large ribosomal subunit—and to cold stress. In fact, several DBRHs have been reported to be involved in acclimation to cold stress. RH7 plays a role in pre-18S rRNA processing and small ribosome subunit biogenesis, and promotes plant development at low temperatures (Huang et al., 2016; Liu et al., 2016). The cytosolic RH5, RH9, and RH25 helicases are involved in the response to both salt and cold stresses (Kant et al., 2007; Kim et al., 2008), whereas the plastid-localized RH3, which is required for intron splicing, mediates salt- and cold-stress responses

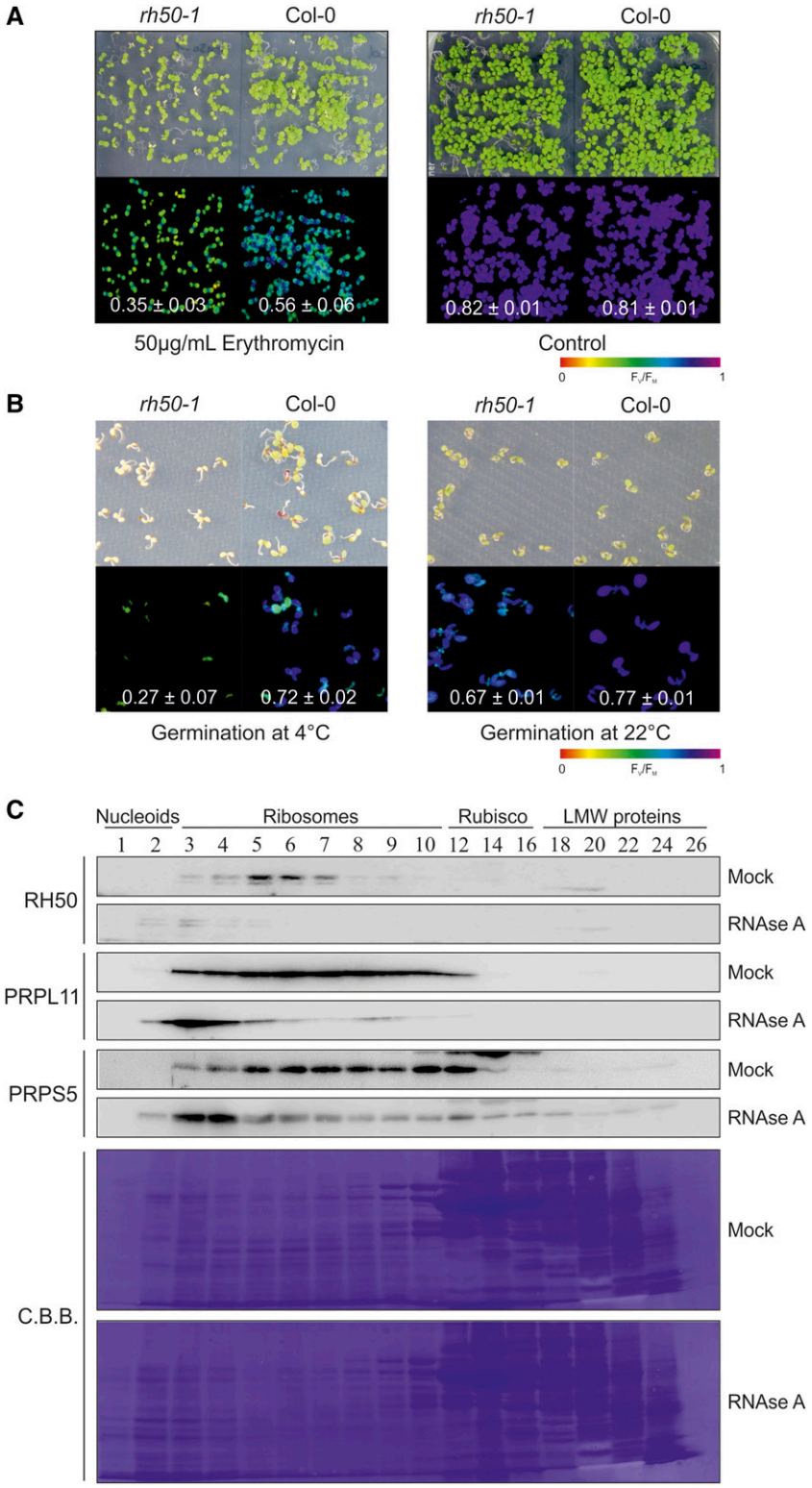

Figure 4. Association of RH50 with chloroplast ribosomes. A, The *rh50-1* mutant is sensitive to erythromycin. Ten-d-old wild-type (Col-0) and *rh50-1* seedlings were germinated on MS containing 50 μg/mL erythromycin (left panel) or on MS plates without antibiotic (right panel). The maximum quantum yield of photosystem II (F_V/F_M) was determined for each condition (average ± SD; $n \geq 12$). The color scale at the bottom indicates the signal intensities. B, The *rh50-1* mutant is cold sensitive. Col-0 and *rh50-1* seedlings were germinated at 4°C (left panel) and 22°C (right panel) and transferred to 22°C for 1 week. The maximum quantum yield of photosystem II (F_V/F_M) was determined for each condition (average ± SD; $n \geq 12$). The color scale at the bottom indicates the signal intensities. Note that the *rh50-1* mutant phenotype becomes only evident in very young plants (until 1 week after germination as in this panel), whereas after 10 d after germination (as in A) the mutant phenotype is recovered. C, RH50 comigrates with ribosomal particles. After fractionation of RNase-treated and untreated wild-type stromal extracts by size-exclusion chromatography, proteins were precipitated, transferred onto PVDF membranes, and immunodecorated with antibodies against RH50, PRPL11, and PRPS5. Note that PRPL11 and PRPS5 accumulate in fractions 3 and 4 when extracts are pretreated with RNase. This might be due to conformational changes induced by partial digestion of the rRNA in mature ribosomes, which makes them less compact, such that they emerge from the column earlier (Jenkins and Barkan, 2001; Meurer et al., 2017). Equal loading is demonstrated by Coomassie Brilliant Blue staining of the membrane. Fractions are indicated at the top and complexes were identified on the basis of Olinares et al. (2010). C.B.B., Coomassie Brilliant Blue; LMW, low molecular weight.

(Larkin et al., 2003; Gu et al., 2014). Moreover, RH50 associates with RNA-containing megadalton complexes that are RNase-sensitive and contain ribosomal proteins, suggesting that RH50 interacts with immature chloroplast ribosomes, possibly as a ribosomal biogenesis factor. These observations are compatible with the comigration of the well-characterized, plastid-localized RH22 with ribosomes (Chi et al., 2012), and with the presence of RH50 in pTACs, which also contain ribosomes (Majeran et al., 2012).

Lack of RH50 Affects Translational Capacity in Chloroplasts

Because the results described above point to a function of RH50 in chloroplast ribosomal biogenesis, the translational capacity of *rh50* chloroplasts was also investigated. To this end, wild-type and *rh50-1* seedlings were exposed to cold treatment and nonstressed conditions as described in Figure 4B and polysome-loading experiments were performed (Fig. 5A; Supplemental Fig. S3). We chose to examine *psaA* mRNA, which is efficiently loaded onto polysomes and hence migrates deep into the Suc gradient (Amann et al., 2004; Meurer et al., 2017). Under nonstressed conditions, loading of *psaA* mRNA onto *rh50* polysomes was indistinguishable from the loading onto wild-type polysomes with the peak fractions 9 to 11 (Supplemental Fig. S3). After cold treatment *psaA* transcripts were clearly shifted toward the low-molecular-weight fractions in wild type and *rh50-1* plants, and the effect was more drastic in *rh50-1* (peak fractions 5 to 8) than in the wild type (peak fractions 7 to 9; Fig. 5A).

Rates of protein synthesis in chloroplasts were then evaluated by in vivo labeling in extracts of wild type, *rh50-1*, *prpl11-1*, and *rh50-1 prpl11-1* plants, because the double mutant displayed a synergistic growth and photosynthesis phenotype. To this end, the rate of incorporation of ^{35}[S]Met into plastid proteins was monitored at the six-leaf rosette stage after 5, 10, and 15 min of light exposure (Fig. 5B). Cytosolic synthesis of nucleus-encoded proteins was chemically inhibited with cycloheximide (see "Materials and Methods"). Total proteins were then extracted, fractionated by SDS-PAGE, and the radioactivity incorporated into D1 and D2 proteins was determined. The overall rate of synthesis observed was slightly reduced in the *rh50-1* and *prpl11-1* single mutants with respect to wild-type plants and, as expected, the double mutant was markedly less active than either parental genotype at all three time points, reaching only 37% of the wild-type incorporation level after 15 min (Fig. 5B).

Taken together, these results confirm that lack of RH50 impairs translation in chloroplasts and exacerbates the impact of the relative loss of the plastid ribosomal protein L11.

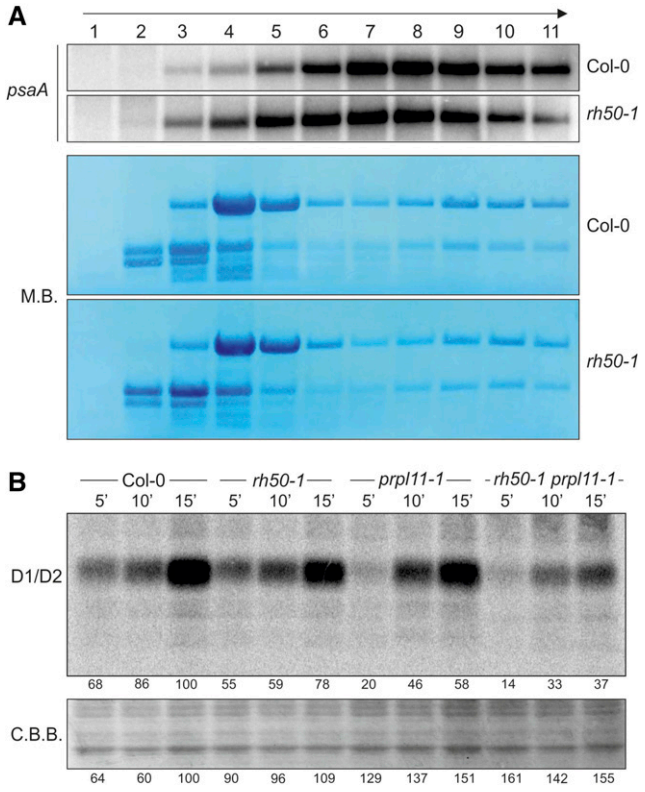

Figure 5. RH50 is required for efficient translation in chloroplasts. A, Polysome loading of the *psaA* mRNA. RNA gel-blot analysis of *psaA* transcripts in polysome fractions 1 to 11 collected after Suc-gradient centrifugation of cold-treated wild-type (Col-0) and *rh50-1* extracts. B, Pulse-labeling analysis of D1/D2 synthesis. Leaves isolated from plants at the 6-leaf rosette stage were pulse-labeled with [^{35}S]Met under low-light illumination (20 μmol photons m^{-2} s^{-1}) for 5, 10, and 15 min in the presence of cycloheximide to inhibit cytosolic protein synthesis. Total leaf proteins were then isolated, fractionated by SDS-PAGE, and detected by autoradiography. A portion of the SDS-PA gel corresponding to the RbcL region was stained with Coomassie Brilliant Blue and served as an internal standard for loading normalization. Quantification of signals (by ImageJ) relative to Col-0 at the 15-min time point (= 100%) is provided below each panel. M.B., Methylene Blue; C.B.B., Coomassie Brilliant Blue.

RH50 Is Involved in Plastid rRNA Metabolism

To investigate the role of RH50 in chloroplast RNA metabolism, RNA-seq analysis was performed on total RNA extracted from 3-week-old wild-type and *rh50-1* plants (Supplemental Table S1; Supplemental Fig. S4). Expression of nuclear genes was largely unaffected in *rh50-1* plants (Supplemental Table S1). However, inspection of chloroplast gene expression revealed a marked increase in levels of transcripts derived from the *rrn23S-rrn4.5S* intergenic region in the mutant, as well as less pronounced changes in 16S rRNA and mRNAs for Rpl2 and Rpl23 (Supplemental Fig. S3; Fig. 6A).

To corroborate the RNA-seq data, accumulation of plastid rRNAs in wild-type (Col-0) and *rh50-1* plants was investigated by RNA blot analyses (Fig. 6, B and C). Plants carrying the *gun1-102* or *gun1-102 rh50-1* mutations were included, because *gun1-102* and *rh50-1* interact with ribosomal mutations in similar ways based on the growth phenotype of resulting double mutants (see Fig. 3). In the wild type, the polycistronic plastid rRNA operon (*rrn16-trnI-trnA-rrn23S-rrn4.5S-rrn5S*) is transcribed as a single RNA molecule and further processed by various nucleases, generating as intermediate products a 16S precursor, a bicistronic 23S-4.5S precursor, and a 5S precursor (Shajani et al., 2011). The 23S-4.5S precursor (3.2 kb) undergoes endonucleolytic cleavage to produce 4.5S (*rrn4.5S*) and 23S RNA (*rrn23S*) fragments (2.9 kb). The 23S precursor is then further processed and eventually gives rise to mature transcripts of 1.3 kb, 1.1 kb, and 0.5 kb in the chloroplast ribosome (Bollenbach et al., 2005). These processing steps and the probes used for RNA gel-blot analyses are summarized

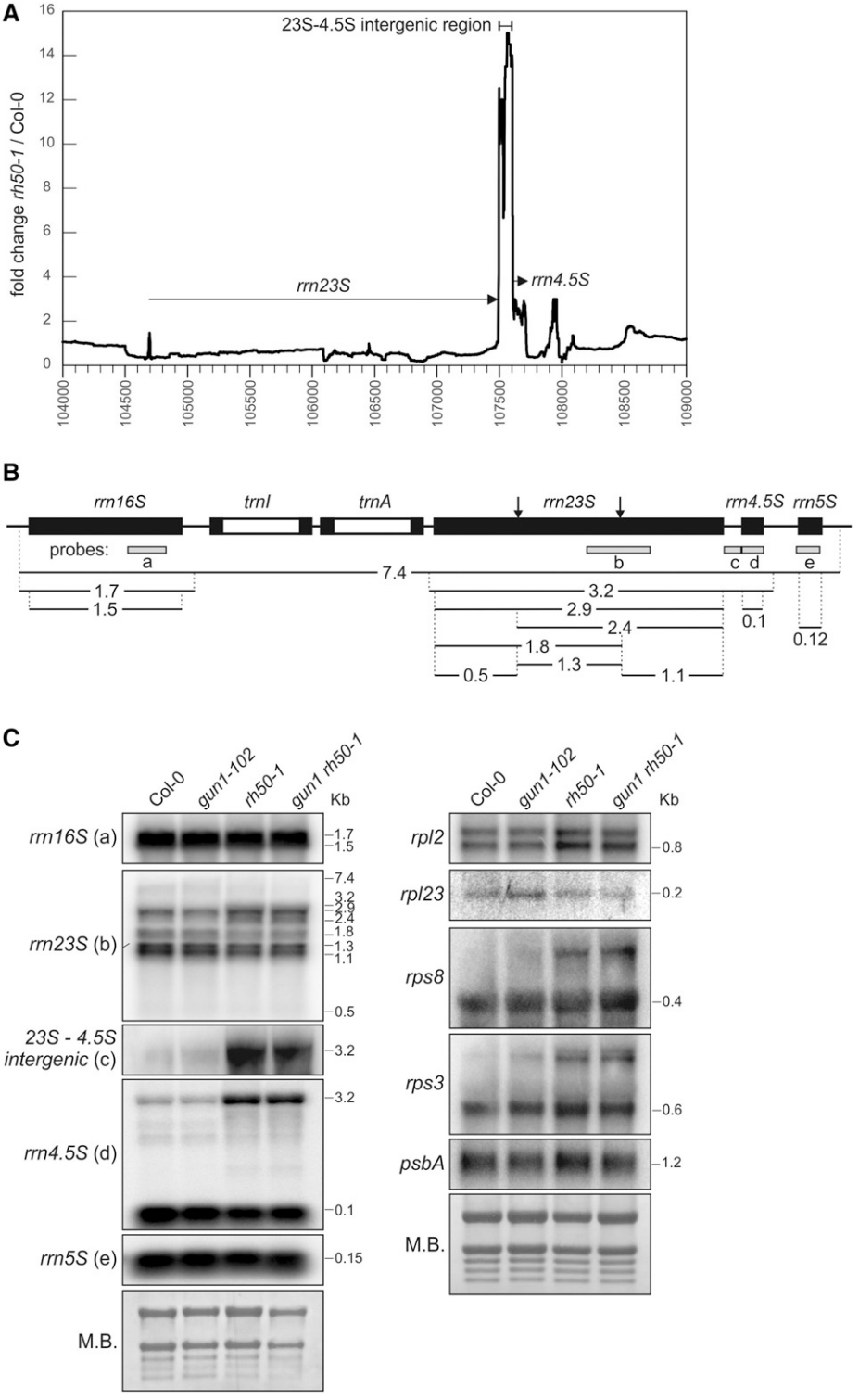

Figure 6. RH50 is required for processing of the *rrn23S-rrn4.5S* rRNA polycistronic transcript. A, Transcripts of the *rrn23S-rrn4.5S* intergenic region are enriched in the *rh50-1* mutant. The fold change between *rh50-1* mutant and wild type (Col-0) in read coverage in the 23S and 4.5S rRNA genomic region is shown, together with a scale model of the gene. *rrn23S*: position 104690 to 107500; *rrn4.5S*: 107598-107701. B, Schematic representation of the chloroplast rRNA operon in Arabidopsis showing the locations of the probes (a to e) used for the northern-blot analysis in (C). All precursors, intermediates, and mature forms with their respective lengths in kilonucleotides are shown. The arrows indicate the position of the hidden breaks; white rectangles represent introns. C, RNA gel-blot analysis with probes specific for plastid rRNAs (16S, 5S, 23S, 4.5S, 23S-4.5S intergenic region, *rpl2*, *rpl23*, *rps8*, *rps3*, and *psbA*) were performed on total RNA isolated from 14-d-old wild-type (Col-0) and mutant (*gun1-102*, *rh50-1*, and *gun1-102 rh50-1*) plants. M.B., Methylene Blue.

in Figure 6B. The data showed that *rrn16S* and *rrn5S* rRNA transcripts (detected with probe a and probe e, respectively; Fig. 6B) accumulate to the same levels in the wild-type and all mutant backgrounds analyzed (Fig. 6C). However, RNA blots hybridized with probes specific for *rrn23S* (probe b) and *rrn4.5S* (probe d) revealed defects in the processing of *rrn23S* and *rrn4.5S* transcripts in the absence of RH50. In both *rh50-1* and *rh50-1 gun1-102* mutants, levels of mature *rrn23S* and *rrn4.5S* transcripts appeared slightly reduced, whereas unprocessed transcripts were enriched relative to wild type and *gun1-102*. RNA blots probed with the 23S-4.5S intergenic

region probe (c) showed only a barely detectable signal in wild type and *gun1-102*, whereas transcripts of this region accumulated approximately 7-fold in *rh50-1* and *gun1-102 rh50-1* mutants (Fig. 6C). These findings strongly suggest that RH50 is required for correct processing of RNA sequences derived from the 23S-4.5S intergenic region. Because the *gun1-102 rh50-1* double mutant behaves like *rh50-1*, GUN1 evidently plays no role in this pathway.

Furthermore, the level of the mature *rpl2* transcript was increased in *rh50-1* and *gun1-102 rh50-1* mutants, confirming the trend found by the RNA-seq analysis, whereas no differences in transcript accumulation were observed for *rpl23*. In the case of *rps8* and *rps3*, processing defects were observed, as increased amounts of the precursor forms were detected in *rh50-1* and *gun1-102 rh50-1* mutants (Fig. 6C) similar to the effects seen for the rRNAs. Because no defect in the steady-state levels of the mature mRNAs was noticed, this is probably a secondary effect of the overall perturbation of the translation machinery (Fristedt et al., 2014). No processing defect was observed for *psbA*.

Taken together, these results imply that maturation of *rrn23S* and *rrn4.5* RNAs is affected in the *rh50-1* mutant, providing a plausible explanation for the impairment of ribosome biogenesis and functionality.

RH50 Associates with the 23S-4.5S Intergenic Region

Because RH50 is required for maturation of the *rrn23S* and *rrn4.5S* RNAs and the processing intermediate *rrn23S-rrn4.5S* strongly accumulates in *rh50-1* (see above), we asked whether RH50 interacts directly with the *rrn23S-rrn4.5S* precursor. To this end, RNA-immunoprecipitation (IP) experiments were performed with wild-type stroma extracts, employing an RH50-specific antibody and the preimmune serum as a control. The specificity of the antibody was checked by a western-blot analysis, which confirmed that it was able to precipitate the RH50 protein (Fig. 7A). Slot-blot analysis of coprecipitated RNAs revealed that the *rrn23S-rrn4.5S* intergenic region was highly enriched in the pellet fraction of the IP performed with anti-RH50 antibodies (ratio pellet/supernatant: 0.80), whereas a control RNA of similar abundance, *rrn16S*, was much less enriched (ratio pellet/supernatant: 0.18; Fig. 7B). To verify that RH50 binds directly to the *rrn23S-rrn4.5S* RNA species, an electrophoretic mobility shift assay (EMSA) was performed utilizing affinity-purified recombinant RH50 protein, a radiolabeled probe for the *rrn23S-rrn4.5S* intergenic region and, as a control, the upstream region adjacent to the *rrn23S* RNA (Fig. 7, C and D). A shift in electrophoretic mobility was only observed for the *rrn23S-rrn4.5S* RNA (Fig. 7D), implying that RH50—like RH22 (which binds to the 5′ region of the 23S rRNA; Chi et al., 2012) and RH39 (that binds to a 23S rRNA segment close to the hidden break; Nishimura et al., 2010)—recognizes a specific rRNA target.

Taken together, our results thus indicate that RH50 promotes the maturation of 23S and 4.5S rRNAs by binding to the *rrn23S-rrn4.5S* intergenic region in the precursor rRNA. We speculate that RH50, as an RNA helicase, unwinds double-stranded segments in this region to facilitate cleavage by a sequence-specific endonuclease.

DISCUSSION

RH50 Promotes Biogenesis of the Plastid Ribosome by Facilitating the Processing of *rrn23S-rrn4.5S* rRNA

Ribosome biogenesis is a complex, multistep process that requires transcription of the ribosomal gene cluster, rRNA processing, and ribosome assembly (Kaczanowska and Rydén-Aulin, 2007). Several factors involved in plastid ribosome biogenesis have been described. Among these, RHON1 was shown to bind the intercistronic region of the *rrn23S-rrn4.5S* RNA precursor and to specify the sequence cleaved by the Arabidopsis endonuclease RNaseE (Stoppel et al., 2012); SUPPRESSOR OF THYLAKOID FORMATION1, a plastid-localized pentatricopeptide repeat protein, is also required for correct processing of 23S-4.5S rRNA precursor (Wu et al., 2016), whereas RAP, an octotricopeptide repeat protein, binds to the 5′ region of the 16S rRNA precursor and promotes its maturation (Kleinknecht et al., 2014). Furthermore, the chloroplast DBRH RH39 plays an essential role in introducing the hidden break into the 23S rRNA, acting together with an as-yet unidentified endonuclease (Nishimura et al., 2010). A second plastid-localized DBRH, RH22, stimulates assembly of the 50S ribosomal subunit by participating in the processing of 23S rRNA and, at the same time, binding to the ribosomal protein PRPL24 (Chi et al., 2012).

In this study, we present multiple lines of evidence for the involvement of a third DBRH, RH50, in chloroplast rRNA metabolism. In *rh50-1* plants, absence of RH50 renders protein synthesis in the chloroplast abnormally sensitive to erythromycin and low temperatures (see Fig. 4), whereas polysome loading is perturbed in cold-acclimated plants and translation efficiency is reduced under standard growth conditions (see Fig. 5). Furthermore, genetic analyses reveal interactions between *rh50-1* and mutations in genes for proteins of the 50S ribosomal subunit (see Fig. 3), and in wild-type plants RH50 associates with ribosomal particles (see Fig. 4). Finally, we show that maturation of the *rrn23S-rrn4.5S* processing intermediate is impaired in *rh50-1* plants (see Fig. 6), and that affinity-purified RH50 binds specifically to the *rrn23S-rrn4.5S* intergenic region, as demonstrated by IP and EMSA experiments (see Fig. 7).

A role for RH50 in rRNA processing can also account for the cold sensitivity of *rh50-1* plants (see Fig. 4B). Several previous studies have suggested that RNA helicases play a pivotal role in plant stress responses (Liu et al., 2002; Owttrim, 2006; Vashisht and Tuteja, 2006; Kant et al., 2007; Nawaz and Kang, 2017). Because these enzymes mediate localized unwinding of RNAs, they might well become critical at low temperatures, which are expected to stabilize RNA secondary structure (Herschlag, 1995; Jones and

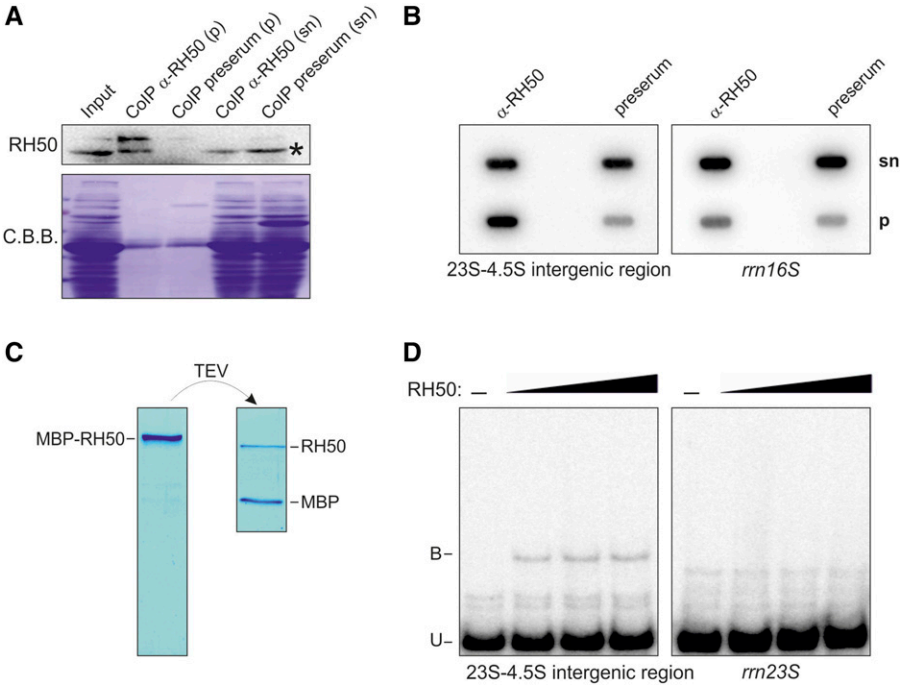

Figure 7. RH50 binds to the *rrn23S-rrn4.5S* intergenic region. A, Western-blot analysis of immunoprecipitated RH50. An antibody specific for RH50 (α-RH50) was used, together with the corresponding preimmune serum (preserum) as a control. Note that the lower band (indicated by an asterisk) is a nonspecific signal. B, Slot-blot analysis of coimmunoprecipitated RNAs. RNAs recovered from the supernatant and the pellet fractions after IP with α-RH50 or the corresponding preimmune serum were applied to a nylon membrane using a slot-blot manifold and hybridized with probes specific for the 23S-4.5S intergenic region or *rrn16S* as control. C, Affinity purification of MBP-RH50 proteins before and after AcTEV cleavage. Purified proteins were stained with Coomassie Brilliant Blue. D, The RNA-binding capacity of the affinity-purified RH50 was analyzed by EMSA using radiolabeled RNA probes for the 23S rRNA and 23S-4.5S intergenic region as indicated. Increasing concentrations of the purified RH50 protein (black triangles) were used for binding experiments. B, bound; U, unbound; P, pellet; sn, supernatant. C.B.B., Coomassie Brilliant Blue.

Inouye, 1996; Lorsch, 2002). In fact, the cytosolic RH7, which is involved in pre-18S rRNA processing and biogenesis of the small (40S) ribosomal subunit, is essential for plant development at low temperatures (Huang et al., 2016; Liu et al., 2016). Moreover, the helicases RH5, RH9, and RH25 contribute to the response to salt and cold stresses (Kant et al., 2007; Kim et al., 2008), and the plastid-located RH3, which is required for intron splicing, mediates salt- and cold-stress responses (Gu et al., 2014).

The Functional Relationship among RH50, GUN1, and Plastid Signaling

GUN1 interacts genetically with *PRPL11* and *PRPS1*, and its product binds to the chloroplast ribosomal protein PRPS1 (Tadini et al., 2016). In this study, these interaction studies were extended by comparing the epistatic effects of *rh50-1* and *gun1-102* on additional mutations affecting chloroplast ribosomal proteins. Clearly, loss of *RH50* and *GUN1* modulates the effects of selected ribosomal mutations in similar ways. Generally speaking, combinations of *rh50-1* or *gun1-102* with *prps17-1*, *prps21*, *prpl11*, or *prpl24* tend to potentiate the phenotypes of the respective single mutants, with *gun1-102* having the more dramatic effect than *rh50-1* when combined with *prps17-1* or *prpl11-1*, and *rh50-1* inducing a stronger effect than loss of *GUN1* in the case of the *prpl24-1* mutation. With respect to the *prps1-1* and *prors1-1* mutations, both *rh50-1* and *gun1-102* act as suppressor mutations (Tadini et al., 2016 and this study). These findings concerning loss of RH50 are consistent with previous observations, which implied that several RNA helicases, specifically RH3, RH39, and RH22, interact with ribosomal proteins (Nishimura et al., 2010; Asakura et al., 2012; Chi et al., 2012).

In addition to the similar behavior of double mutants that lack either RH50 or GUN1, there are additional similarities between the two genes and their mutants. In fact, *RH50* is coregulated with *GUN1* (see Fig. 1A). RH50 and GUN1 are located in the same subcompartment (see Fig. 1B), and *rh50-1*—like *gun1-102* (Tadini et al., 2016)—suppresses the down-regulation of PhANG expression seen in the *prors1-1* mutant (see Fig. 2D). However, unlike *gun1-102*, *rh50-1* itself does not induce the classical *gun* phenotype observed in seedlings exposed to NF or LIN (see Fig. 2C). So, what can we learn from these results with respect to the function of GUN1? Based on the similarities of GUN1 and RH50

outlined above and our finding that RH50 has a role in rRNA metabolism and appears to interact with immature plastid ribosomes (Figs. 4 to 7), it is tempting to speculate that also GUN1 has a function that is related to ribosome biogenesis or its functionality. But clearly, the mechanism by which GUN1 exerts this function differs from that of RH50, because GUN1 appears to bind proteins rather than RNAs (Tadini et al., 2016).

CONCLUSIONS

RH50 is a plastid rRNA maturation factor that possibly interacts with immature ribosomes, and consequently its absence affects the functionality of ribosomes. The similarities between RH50 and GUN1, in particular with respect to the behavior of their mutants, allows us to speculate that GUN1 might also have a function in plastid ribosome biogenesis and functionality. Future studies aimed to clarify the function of GUN1, and its interplay with ribosome biogenesis might take advantage of the observed double mutant phenotypes observed in this study, for instance by designing genetic suppressor screens to identify mutations that behave like *gun1* in suitable double mutants.

MATERIALS AND METHODS

Plant Material, Propagation, and Growth Measurements

The Arabidopsis (*Arabidopsis thaliana*) T-DNA insertion mutant line *rh50-1* (GABI_629A10, genetic background Col-0) was obtained from the GABI-KAT collection (Rosso et al., 2003) and the transposon line *rh50-2* (GT_5_111858, genetic background L*er*) from the GT collection (http://gt.jbei.org/arabidopsis.html). The regions flanking the insertions were PCR-amplified and sequenced (primer sequences in Supplemental Table S2), and both the T-DNA and the transposon were found to lie in exon 2 (at positions 433 and 429 relative to the start codon, respectively). In addition, the following previously described mutant lines were used in this work: *gun1-102* and *prps21-1* (Tadini et al., 2016), *prors1-1* (Pesaresi et al., 2006), *prpl11-1* (Pesaresi et al., 2001), and *prps1-1*, *prps17-1*, and *prpl24-1* (Romani et al., 2012).

Arabidopsis plants were grown on soil in a climate chamber as described (Pesaresi et al., 2009). For treatment with NF or antibiotics, surface-sterilized mutant and wild-type seeds were plated on MS medium (PhytoTechnology Laboratories) containing 1% (w/v) Suc and 0.8% (w/v) agar supplemented with either 5 μM NF (Sandoz Pharmaceuticals), 220 μg mL^{-1} LIN (Sigma-Aldrich), 50 μg mL^{-1} erythromycin (Sigma-Aldrich), or 40 μg mL^{-1} chloramphenicol (Sigma-Aldrich). For the cold stress treatments, surface-sterilized mutant and wild-type seeds were plated on MS medium containing 1% (w/v) Suc. The seeds were allowed to germinate in a climate chamber at 4°C under long-day conditions (16 h light/8 h dark) and either standard levels of light or low light (100 or 30 μmol photons s^{-1} m^{-1}) for 6 weeks and then transferred at 22°C under same long-day conditions.

For growth measurements, leaf area was determined with the ImageJ software (http://imagej.nih.gov/ij/index.html).

Transient Coexpression of *GUN1* and *RH50* cDNAs in Arabidopsis Leaf Protoplasts

GUN1 and *RH50* cDNA were cloned without their stop codons into the Gateway entry vector pDONR207 (Invitrogen) as described (Tadini et al., 2016). The entry vector was then recombined with pK7RWG2 and pB7FWG2 (Vinti et al., 2000) to generate 35S promoter-driven C-terminal GUN1-RFP and RH50-GFP fusions.

Two-week-old wild-type Arabidopsis seedlings were cut into small pieces and incubated for 16 h at 24°C in the dark in a protoplasting solution (10 mM MES, 20 mM $CaCl_2$, 0.5 M mannitol, pH 5.8, containing 0.1 g mL^{-1} macerozyme and 0.1 g mL^{-1} cellulase; Duchefa). Protoplasts were then isolated as described previously (Dovzhenko et al., 2003) and transfected with the GUN1-RFP and RH50-GFP constructs by the calcium-PEG method. Protoplasts were incubated for 24 h, and then assessed for fusion gene expression with a confocal microscope (TCS SP5 CLSM; Leica).

Chlorophyll *a* Fluorescence Measurements

Five plants of each genotype were analyzed, and average values and SDs were calculated. In vivo chlorophyll *a* fluorescence of single leaves was measured using the Dual-PAM 100 (Walz). Pulses (0.5 s) of saturating light (5000 μmol photons m^{-2} s^{-1}) were used to determine the maximum fluorescence (F_M) and the ratio $(F_M - F_0)/F_M = F_V/F_M$, where F_0 is the minimum fluorescence. A 15-min exposure to actinic light (37 μmol photons m^{-2} s^{-1}) was used to drive electron transport before measuring Φ_{II} (Armbruster et al., 2010). In vivo Chl *a* fluorescence of whole plants was recorded using an imaging Chl fluorometer (Imaging PAM; Walz, Germany). Dark-adapted plants were exposed to a pulsed, blue measuring beam (1 Hz, intensity 4; F_0) and a saturating light flash (intensity 4) to obtain F_V/F_M.

Coexpression Analysis

To identify genes represented on the ATH1 Affymetrix microarray (22 K) chip that show a significant degree of coexpression with *GUN1*, an expression correlation analysis was performed with the CoExSearch tool implemented in ATTED-II (http://atted.jp/; Obayashi et al., 2007; Obayashi et al., 2009). Hierarchical clustering was done with the single-linkage method using the HCluster tool in ATTED-II.

Transcriptome Sequencing and Analysis

Total RNA was extracted from 3-week-old wild-type and *rh50-1* plants, using standard TRIzol extraction. RNA was tested for quality by spectrophotometry, agarose gel electrophoresis, and PCR. RNA-Seq library preparation and long noncoding RNA sequencing were both performed at Novogene Biotech using standard Illumina protocols. The RNA-Seq libraries were sequenced using the paired-end mode on an Illumina HiSEquation 2500 system. At least three biological replicates were used for each analysis.

The quality of the raw data were verified with FASTQC (http://www.bioinformatics.babraham.ac.uk/projects/fastqc/). Sequences were filtered and trimmed using Trimmomatic (http://www.usadellab.org/cms/?page=trimmomatic; Bolger et al., 2014). Reads were mapped to the Arabidopsis reference genome (TAIR10) using HISAT with default parameter settings (https://ccb.jhu.edu/software/hisat/index.shtml). Transcript assembly and FPKM (RPKM) values were calculated using htseq-count (http://htseq.readthedocs.io/en/release_0.9.1/, version of 2016). Deregulated genes were identified with DESeq2 (https://bioconductor.org/packages/release/bioc/html/DESeq2.html; Love et al., 2014). All of these analyses were performed using a local Galaxy server (http://galaxyproject.org; Giardine et al., 2005).

To obtain a more detailed view of the chloroplast genome, the reads from wild type and *rh50-1* were mapped to the chloroplast genome of Arabidopsis using Qiagen's CLC Genomics Workbench v.8.5.1 (hereafter, CLC). Before assembly, the reads were trimmed using CLC with default settings. The trimmed sequences were then mapped to the chloroplast genome of Arabidopsis (NC_000932.1). Fold changes were calculated and visualized with Excel (Microsoft).

Nucleic Acid Analysis

Arabidopsis genomic DNA was isolated as described (Ihnatowicz et al., 2004) and RNA was purified from frozen leaf tissue as described before (Armbruster et al., 2010). RNA gel-blot analyses were performed under stringent conditions (Green and Sambrook, 2012) using 5-μg samples of total RNA. Primers used to amplify the probes are listed in Supplemental Table S2. cDNA fragments were used, except in the case of the 23S-4.5S rRNA intergenic region, for which 5′-end ^{32}P-labeled ssDNA was employed. Signals were quantified with the ImageJ software (http://imagej.nih.gov/ij/index.html).

Immunoblot Analyses

Immunoblot analyses were carried out as described (Ihnatowicz et al., 2004), using antibodies directed against GFP (Life Technologies), RbcL (Agrisera), PRPS1

(Agrisera), PRPS5 (Agrisera), PRPL11 (Meurer et al., 2017), or RH50 (GenScript). The RH50 antibody was raised against the peptide CDNERGLRGGSHSKG. Signals were quantified with ImageJ software.

Y2H and Polysome Analyses

For Y2H assays, the coding sequences of the mature proteins (without the chloroplast transit peptides cTP) of interest (see Supplemental Table S2 for primer sequences) were cloned into pGBKT7 (RH50) and pGADT7 (GUN1, PRPS21, PRPS17, PRPL11, and PRPL24) vectors (Clontech), or vice versa. Interactions in yeast were then analyzed as described before (DalCorso et al., 2008).

Polysome loading experiments were conducted as described (Barkan, 1993).

In Vivo Translation Assay

The in vivo translation assay was performed essentially as described previously (Tadini et al., 2016). Twelve leaf discs (4-cm diameter) were incubated in a buffer containing 20 μg mL^{-1} cycloheximide, 1 mM K_2HPO_4/KH_2PO_4 (pH 6.3), and 0.1% (w/v) TWEEN 20 to block cytosolic translation. Then [^{35}S]Met was added to the buffer (0.1 mCi mL^{-1}) and the material was vacuum-infiltrated. Leaves were exposed to light (20 μmol photons m^{-2} s^{-1}) and four leaf discs were collected at each time point (5, 15, and 30 min). Total proteins were extracted as described (Martínez-García et al., 1999) and loaded on Gly SDS-PA (12% PAA) gels. Signals were detected and quantified using a PhosphoImager (GE Healthcare Life Sciences; www3.gehealthcare.com) and the program Image Quant (GE Healthcare Life Sciences).

Co-IP and Slot-Blot Analysis

Chloroplasts from 3-week-old wild-type plants were isolated as described previously (Stoppel et al., 2012). Lysis was achieved by passing the chloroplast-containing solution (30 mM HEPES pH 8.0, 10 mM Mg acetate, 60 mM K acetate, freshly added Protease Inhibitor Cocktail [Roche]) through a 0.45-mm needle 25 times. Lysates were cleared by centrifugation at 45,000*g* for 30 min at 4°C. Samples (each equivalent to 1 mg of stroma) were diluted with the same volume of Co-IP buffer (20 mM Tris pH 7.5, 150 mM NaCl, 1 mM EDTA, 0.5% Nonidet P40, Protease Inhibitor Cocktail; Roche) and incubated either with RH50-specific antibodies (30 μL) or with the corresponding preserum (2 μL) for 1 h at 4°C, and then with 50 μL of SiMAG-Protein G beads (Chemicell) for a further hour. Washing, RNA extraction and slot-blot analysis were performed as described previously (Meurer et al., 2017)

Production of Recombinant RH50 and Its Use in EMSA

The *RH50* sequence encoding the mature RH50 protein was cloned into the *Bam*HI-*Sal*I sites of the pMAL-Tev vector. The coding sequence for Strep-Tag (WSHPQFEK) was added to the reverse primer (see Supplemental Table S2 for primer sequences). The pMAL-Tev vector was kindly provided by Alice Barkan. Expression, affinity purification, and proteolytic digestion were conducted as described previously (Chi et al., 2014).

The EMSA experiments were performed essentially as described previously (Meurer et al., 2017). Increasing concentrations of recombinant RH50 (100 nM, 200 nM, and 400 nM) were used.

Size Exclusion Chromatography

Size exclusion chromatography of stroma isolated from 3-week-old plants was conducted as described (Meurer et al., 2017). Three mg of stroma extracts were used.

Accession Numbers

The genes coexpressed with *RH50* code for: RH11, DEAD-box ATP-dependent RNA helicase 11 (*At3g58510*); (*At4g01690*); RH17, DEAD-box ATP-dependent RNA helicase 17 (*At2g40700*); RH22, DEAD-box ATP-dependent RNA helicase 22 (*At1g59990*); RH26, DEAD-box ATP-dependent RNA helicase (*At5g08610*); RH52, DEAD-box ATP-dependent RNA helicase 52 (*At3g58570*); RH58, DEAD-box ATP-dependent RNA helicase 58 (*At5g19210*); GUN1, Genomes Uncoupled 1 (*At2g31400*); PRPS1, plastid ribosomal protein S1 (*At5g30510*); CHLD, magnesium chelatase subunit D (*At1g08520*); PPOX, protoporphyrinogen oxidase.

The genes analyzed by northern blotting, size-exclusion chromatography, and polysome fractionation were: *rrn16S* (*AtCg00920*), *rrn23S* (*AtCg01180*), *rrn4.5S* (*AtCg00960*), *rrn5S* (*AtCg00970*), *rbcL* (*AtCg00490*), *psbA* (*AtCg00020*), *LHCA3* (*At1g61520*), *LHCA4* (*At3g47470*), *LHCB1.2* (*At1g29910*), *LHCB4.1* (*At5g01530*), *PSAE1* (*At4g28750*), *PSAK* (*At1g30380*), *PSAO* (*At1g08380*), *PSAD1* (*At4g02770*), *psaA* (*AtCg00350*), *rpl2.1* (*AtCg00830*), *rpl23.1*(*AtCg00840*), *rps8* (*AtCg00770*), *PRPS3* (*At3g07040*).

The following proteins were analyzed by Y2H: PRPS1, GUN1, CHLD (see above), RH50 (At3g06980), PRPS21 (At3g27160), PRPL11 (At1g32990), PRPL24 (At5g54600), PRPS17(At1g79850).

Supplemental Data

The following supplemental materials are available.

Supplemental Figure S1. The *rh50-1* mutant is sensitive to cold stress.

Supplemental Figure S2. Characterization of protein interactions of RH50.

Supplemental Figure S3. Polysome loading of the *psaA* mRNA under normal growth conditions.

Supplemental Figure S4. Differential enrichment of chloroplastic RNAs.

Supplemental Table S1. Differentially expressed genes obtained from RNA-seq analysis.

Supplemental Table S2. Primers used in this study.

ACKNOWLEDGMENTS

The authors thank Paul Hardy for critical reading of the manuscript.

Received October 26, 2017; accepted November 11, 2017; published November 14, 2017.

LITERATURE CITED

Amann K, Lezhneva L, Wanner G, Herrmann RG, Meurer J (2004) ACCUMULATION OF PHOTOSYSTEM ONE1, a member of a novel gene family, is required for accumulation of [4Fe-4S] cluster-containing chloroplast complexes and antenna proteins. Plant Cell **16:** 3084–3097

Armbruster U, Zühlke J, Rengstl B, Kreller R, Makarenko E, Rühle T, Schünemann D, Jahns P, Weisshaar B, Nickelsen J, Leister D (2010) The *Arabidopsis* thylakoid protein PAM68 is required for efficient D1 biogenesis and photosystem II assembly. Plant Cell **22:** 3439–3460

Asakura Y, Galarneau E, Watkins KP, Barkan A, van Wijk KJ (2012) Chloroplast RH3 DEAD box RNA helicases in maize and *Arabidopsis* function in splicing of specific group II introns and affect chloroplast ribosome biogenesis. Plant Physiol **159:** 961–974

Barkan A (1993) Nuclear mutants of maize with defects in chloroplast polysome assembly have altered chloroplast RNA metabolism. Plant Cell **5:** 389–402

Bolger AM, Lohse M, Usadel B (2014) Trimmomatic: a flexible trimmer for Illumina sequence data. Bioinformatics **30:** 2114–2120

Bollenbach TJ, Lange H, Gutierrez R, Erhardt M, Stern DB, Gagliardi D (2005) RNR1, a 3′-5′ exoribonuclease belonging to the RNR superfamily, catalyzes 3′ maturation of chloroplast ribosomal RNAs in *Arabidopsis thaliana*. Nucleic Acids Res **33:** 2751–2763

Caruthers JM, McKay DB (2002) Helicase structure and mechanism. Curr Opin Struct Biol **12:** 123–133

Chi W, He B, Manavski N, Mao J, Ji D, Lu C, Rochaix JD, Meurer J, Zhang L (2014) RHON1 mediates a Rho-like activity for transcription termination in plastids of *Arabidopsis thaliana*. Plant Cell **26:** 4918–4932

Chi W, He B, Mao J, Li Q, Ma J, Ji D, Zou M, Zhang L (2012) The function of RH22, a DEAD RNA helicase, in the biogenesis of the 50S ribosomal subunits of *Arabidopsis* chloroplasts. Plant Physiol **158:** 693–707

Cordin O, Banroques J, Tanner NK, Linder P (2006) The DEAD-box protein family of RNA helicases. Gene **367:** 17–37

DalCorso G, Pesaresi P, Masiero S, Aseeva E, Schünemann D, Finazzi G, Joliot P, Barbato R, Leister D (2008) A complex containing PGRL1 and PGR5 is involved in the switch between linear and cyclic electron flow in *Arabidopsis*. Cell **132:** 273–285

Dovzhenko A, Dal Bosco C, Meurer J, Koop HU (2003) Efficient regeneration from cotyledon protoplasts in *Arabidopsis thaliana*. Protoplasma **222:** 107–111

Fristedt R, Scharff LB, Clarke CA, Wang Q, Lin C, Merchant SS, Bock R (2014) RBF1, a plant homolog of the bacterial ribosome-binding factor RbfA, acts in processing of the chloroplast 16S ribosomal RNA. Plant Physiol **164:** 201–215

Giardine B, Riemer C, Hardison RC, Burhans R, Elnitski L, Shah P, Zhang Y, Blankenberg D, Albert I, Taylor J, Miller W, Kent WJ, et al (2005) Galaxy: a platform for interactive large-scale genome analysis. Genome Res **15:** 1451–1455

Green MR, Sambrook J (2012) Molecular Cloning: A Laboratory Manual. Cold Spring Harbor Laboratory Press, Cold Spring Harbor, NY

Gu L, Xu T, Lee K, Lee KH, Kang H (2014) A chloroplast-localized DEAD-box RNA helicase AtRH3 is essential for intron splicing and plays an important role in the growth and stress response in *Arabidopsis thaliana*. Plant Physiol Biochem **82:** 309–318

Herschlag D (1995) RNA chaperones and the RNA folding problem. J Biol Chem **270:** 20871–20874

Huang C-K, Shen Y-L, Huang L-F, Wu S-J, Yeh C-H, Lu C-A (2016) The DEAD-Box RNA helicase AtRH7/PRH75 participates in Pre-rRNA processing, plant development and cold tolerance in *Arabidopsis*. Plant Cell Physiol **57:** 174–191

Ihnatowicz A, Pesaresi P, Varotto C, Richly E, Schneider A, Jahns P, Salamini F, Leister D (2004) Mutants for photosystem I subunit D of *Arabidopsis thaliana*: effects on photosynthesis, photosystem I stability and expression of nuclear genes for chloroplast functions. Plant J **37:** 839–852

Jarmoskaite I, Russell R (2011) DEAD-box proteins as RNA helicases and chaperones. Wiley Interdiscip Rev RNA **2:** 135–152

Jarmoskaite I, Russell R (2014) RNA helicase proteins as chaperones and remodelers. Annu Rev Biochem **83:** 697–725

Jenkins BD, Barkan A (2001) Recruitment of a peptidyl-tRNA hydrolase as a facilitator of group II intron splicing in chloroplasts. EMBO J **20:** 872–879

Jones PG, Inouye M (1996) RbfA, a 30S ribosomal binding factor, is a cold-shock protein whose absence triggers the cold-shock response. Mol Microbiol **21:** 1207–1218

Kaczanowska M, Rydén-Aulin M (2007) Ribosome biogenesis and the translation process in *Escherichia coli*. Microbiol Mol Biol Rev **71:** 477–494

Kant P, Kant S, Gordon M, Shaked R, Barak S (2007) STRESS RESPONSE SUPPRESSOR1 and STRESS RESPONSE SUPPRESSOR2, two DEAD-box RNA helicases that attenuate *Arabidopsis* responses to multiple abiotic stresses. Plant Physiol **145:** 814–830

Kim JS, Kim KA, Oh TR, Park CM, Kang H (2008) Functional characterization of DEAD-box RNA helicases in *Arabidopsis thaliana* under abiotic stress conditions. Plant Cell Physiol **49:** 1563–1571

Kleinknecht L, Wang F, Stübe R, Philippar K, Nickelsen J, Bohne A-V (2014) RAP, the sole octotricopeptide repeat protein in *Arabidopsis*, is required for chloroplast 16S rRNA maturation. Plant Cell **26:** 777–787

Koussevitzky S, Nott A, Mockler TC, Hong F, Sachetto-Martins G, Surpin M, Lim J, Mittler R, Chory J (2007) Signals from chloroplasts converge to regulate nuclear gene expression. Science **316:** 715–719

Larkin RM, Alonso JM, Ecker JR, Chory J (2003) GUN4, a regulator of chlorophyll synthesis and intracellular signaling. Science **299:** 902–906

Li D, Liu H, Zhang H, Wang X, Song F (2008) OsBIRH1, a DEAD-box RNA helicase with functions in modulating defence responses against pathogen infection and oxidative stress. J Exp Bot **59:** 2133–2146

Liu HY, Nefsky BS, Walworth NC (2002) The Ded1 DEAD box helicase interacts with Chk1 and Cdc2. J Biol Chem **277:** 2637–2643

Liu Y, Tabata D, Imai R (2016) A cold-inducible DEAD-box RNA helicase from *Arabidopsis thaliana* regulates plant growth and development under low temperature. PLoS One **11:** e0154040

Lorsch JR (2002) RNA chaperones exist and DEAD box proteins get a life. Cell **109:** 797–800

Love MI, Huber W, Anders S (2014) Moderated estimation of fold change and dispersion for RNA-seq data with DESeq2. Genome Biol **15:** 550

Majeran W, Friso G, Asakura Y, Qu X, Huang M, Ponnala L, Watkins KP, Barkan A, van Wijk KJ (2012) Nucleoid-enriched proteomes in developing plastids and chloroplasts from maize leaves: a new conceptual framework for nucleoid functions. Plant Physiol **158:** 156–189

Martínez-García JF, Monte E, Quail PH (1999) A simple, rapid and quantitative method for preparing *Arabidopsis* protein extracts for immunoblot analysis. Plant J **20:** 251–257

Meurer J, Schmid LM, Stoppel R, Leister D, Brachmann A, Manavski N (2017) PALE CRESS binds to plastid RNAs and facilitates the biogenesis of the 50S ribosomal subunit. Plant J **92:** 400–413

Mingam A, Toffano-Nioche C, Brunaud V, Boudet N, Kreis M, Lecharny A (2004) DEAD-box RNA helicases in *Arabidopsis thaliana*: establishing a link between quantitative expression, gene structure and evolution of a family of genes. Plant Biotechnol J **2:** 401–415

Nawaz G, Kang H (2017) Chloroplast- or mitochondria-targeted DEAD-box RNA helicases play essential roles in organellar RNA metabolism and abiotic stress responses. Front Plant Sci **8:** 871

Nishimura K, Ashida H, Ogawa T, Yokota A (2010) A DEAD box protein is required for formation of a hidden break in *Arabidopsis* chloroplast 23S rRNA. Plant J **63:** 766–777

Obayashi T, Hayashi S, Saeki M, Ohta H, Kinoshita K (2009) ATTED-II provides coexpressed gene networks for *Arabidopsis*. Nucleic Acids Res **37:** D987–D991

Obayashi T, Kinoshita K, Nakai K, Shibaoka M, Hayashi S, Saeki M, Shibata D, Saito K, Ohta H (2007) ATTED-II: a database of co-expressed genes and cis elements for identifying co-regulated gene groups in *Arabidopsis*. Nucleic Acids Res **35:** D863–D869

Olinares PD, Ponnala L, van Wijk KJ (2010) MegaDalton complexes in the chloroplast stroma of *Arabidopsis thaliana* characterized by size exclusion chromatography, mass spectrometry, and hierarchical clustering. Mol Cell Proteomics **9:** 1594–1615

Owttrim GW (2006) RNA helicases and abiotic stress. Nucleic Acids Res **34:** 3220–3230

Pesaresi P, Hertle A, Pribil M, Kleine T, Wagner R, Strissel H, Ihnatowicz A, Bonardi V, Scharfenberg M, Schneider A, Pfannschmidt T, Leister D (2009) Arabidopsis STN7 kinase provides a link between short- and long-term photosynthetic acclimation. Plant Cell **21:** 2402–2423

Pesaresi P, Masiero S, Eubel H, Braun H-P, Bhushan S, Glaser E, Salamini F, Leister D (2006) Nuclear photosynthetic gene expression is synergistically modulated by rates of protein synthesis in chloroplasts and mitochondria. Plant Cell **18:** 970–991

Pesaresi P, Varotto C, Meurer J, Jahns P, Salamini F, Leister D (2001) Knock-out of the plastid ribosomal protein L11 in *Arabidopsis*: effects on mRNA translation and photosynthesis. Plant J **27:** 179–189

Rogalski M, Schöttler MA, Thiele W, Schulze WX, Bock R (2008) Rpl33, a nonessential plastid-encoded ribosomal protein in tobacco, is required under cold stress conditions. Plant Cell **20:** 2221–2237

Romani I, Tadini L, Rossi F, Masiero S, Pribil M, Jahns P, Kater M, Leister D, Pesaresi P (2012) Versatile roles of Arabidopsis plastid ribosomal proteins in plant growth and development. Plant J **72:** 922–934

Rosso MG, Li Y, Strizhov N, Reiss B, Dekker K, Weisshaar B (2003) An *Arabidopsis thaliana* T-DNA mutagenized population (GABI-Kat) for flanking sequence tag-based reverse genetics. Plant Mol Biol **53:** 247–259

Shajani Z, Sykes MT, Williamson JR (2011) Assembly of bacterial ribosomes. Annu Rev Biochem **80:** 501–526

Silverman E, Edwalds-Gilbert G, Lin R-J (2003) DExD/H-box proteins and their partners: helping RNA helicases unwind. Gene **312:** 1–16

Sohmen D, Harms JM, Schlünzen F, Wilson DN (2009) SnapShot: antibiotic inhibition of protein synthesis I. Cell **138:** 1248.e1

Stoppel R, Manavski N, Schein A, Schuster G, Teubner M, Schmitz-Linneweber C, Meurer J (2012) RHON1 is a novel ribonucleic acid-binding protein that supports RNase E function in the *Arabidopsis* chloroplast. Nucleic Acids Res **40:** 8593–8606

Sun X, Xu D, Liu Z, Kleine T, Leister D (2016) Functional relationship between mTERF4 and GUN1 in retrograde signaling. J Exp Bot **67:** 3909–3924

Tadini L, Pesaresi P, Kleine T, Rossi F, Guljamow A, Sommer F, Mühlhaus T, Schroda M, Masiero S, Pribil M, Rothbart M, Hedtke B, et al (2016) GUN1 controls accumulation of the plastid ribosomal protein S1 at the protein level and interacts with proteins involved in plastid protein homeostasis. Plant Physiol **170:** 1817–1830

Vashisht AA, Tuteja N (2006) Stress responsive DEAD-box helicases: a new pathway to engineer plant stress tolerance. J Photochem Photobiol B **84:** 150–160

Vinti G, Hills A, Campbell S, Bowyer JR, Mochizuki N, Chory J, López-Juez E (2000) Interactions between *hy1* and *gun* mutants of *Arabidopsis*, and their implications for plastid/nuclear signalling. Plant J **24:** 883–894

Wang S, Bai G, Wang S, Yang L, Yang F, Wang Y, Zhu J-K, Hua J (2016) Chloroplast RNA-binding protein RBD1 promotes chilling tolerance through 23S rRNA processing in *Arabidopsis*. PLoS Genet **12:** e1006027

Wang Y, Duby G, Purnelle B, Boutry M (2000) Tobacco VDL gene encodes a plastid DEAD box RNA helicase and is involved in chloroplast differentiation and plant morphogenesis. Plant Cell **12:** 2129–2142

Wu W, Liu S, Ruwe H, Zhang D, Melonek J, Zhu Y, Hu X, Gusewski S, Yin P, Small ID, Howell KA, Huang J (2016) SOT1, a pentatricopeptide repeat protein with a small MutS-related domain, is required for correct processing of plastid 23S-4.5S rRNA precursors in *Arabidopsis thaliana*. Plant J **85:** 607–621

Yin T, Pan G, Liu H, Wu J, Li Y, Zhao Z, Fu T, Zhou Y (2012) The chloroplast ribosomal protein L21 gene is essential for plastid development and embryogenesis in *Arabidopsis*. Planta **235:** 907–921

Zhang J, Yuan H, Yang Y, Fish T, Lyi SM, Thannhauser TW, Zhang L, Li L (2016) Plastid ribosomal protein S5 is involved in photosynthesis, plant development, and cold stress tolerance in *Arabidopsis*. J Exp Bot **67:** 2731–2744